ASEAN Engineering Journal

Full Paper

DESIGN AND SIMULATION OF A COMPACT LINE INSPECTION ROBOT

Mark James Ferrer, Jeongrok Lee, Marc Heinz Linsangan, Nygel Gian Santillan*, Matthew Sybingco, Alvin Chua

Department of Mechanical Engineering, Gokongwei College of Engineering, De La Salle University, Manila, Philippines

Article history
Received
27 July 2023
Received in revised form
25 November 2023
Accepted
28 January 2024
Published online
30 November 2024

*Corresponding author
nygel_santillan@dlsu.edu.ph

Graphical abstract

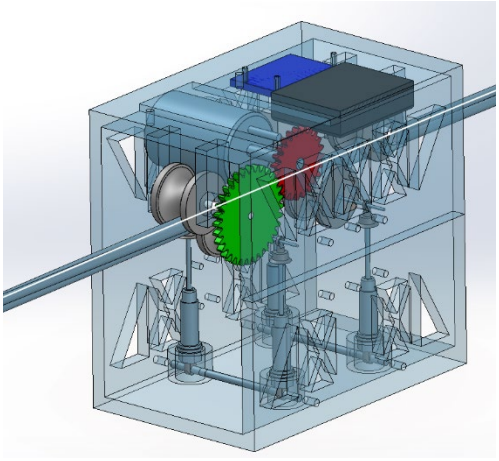

Abstract

Power line inspection is a rather risky and complex task. As a result, robots have been introduced that perform power line inspections with minimal human interaction with the power line itself. Most current designs, however, are unsuited for use in residential powerlines due to their architecture. The study aims to present a compact and lightweight design capable of inspecting residential power lines using a clamshell design. Several elements of the design were designed with the premise that these would be 3D printed to reduce weight and save costs. The study focused on designing several chassis models and different wheel designs. These were run through software such as ANSYS and SOLIDWORKS to determine their structural integrity and ability to traverse the power line respectively. After running tests, it was found that a thin rectangular chassis design with U-type grooved wheels yielded the best results in terms of overall performance, with the highest equivalent stress of 6.484e5 Pa for the individual top chassis and a highest equivalent stress of 3.363e6 Pa found in the wheel axel when an assembly simulation was performed. This resulted in a safety factor of 15 in the stress simulations. Stable behavior was observed in the motion analysis, indicating that the design was feasible for performing an inspection. The design was then modified to reduce print time along with incorporating a specific print setting that yielded a total print time of just over 1 day and an equivalent mass of under 1.5 kg with no relative effect on the structural integrity and stability of the robot.

Keywords: Clamshell design, Wire-riding robot, Motion analysis, Stress analysis, 3D printing

1.0 INTRODUCTION

The inspection of power lines is an important part of power grid maintenance [1]. While power lines are designed to last many years without replacement, frequent inspection is important to detect problems, allowing for swift reactions. The inability to frequently inspect power lines could lead to a failure in the power pole and damage to the power infrastructure. There is also a possibility of people being hurt or electrocuted by a faulty power line.

On average, electric shocks have killed 1,000 citizens each year in the US. This accounts for 1 % of all accidental deaths [2]. Inspecting electric components and systems is known to cause severe burns or other injuries. The elevation of the power lines is another way an accident can occur. It is another hazard as there is the risk of falling if the safety equipment fails. That is why only a licensed electrician should inspect the lines. This risk is amplified for people working in the field of electrical inspection who are constantly exposed to electrical wires that may or may not have been compromised. A power line inspecting robot has the potential to keep workers away from harm when inspecting a power line.

According to an article [3], in the present situation, the technology for power line inspection uses data capture devices from helicopters, cameras, and sensor systems to capture different data. Different technologies such as thermal imagery LiDAR (light distancing and ranging). Which creates a 3D map of the physical world and hyperspectral imagery that uses multiple lights with different wavelengths to identify plant species. Because of the size and weight of this equipment, multiple round

trips were needed to acquire all the necessary data from the different data points, which adds up to the cost. Another technology being used today are unmanned aerial vehicles (UAVs) and drones. Drones such as those presented in [4], [5] show the applicability of drones in the field of power line inspection. These are used with advanced cameras to better cover large sites for faster and easier productivity.

A particular type of robot being researched are Power Transmission Line Inspection Robots. These robots climb onto the transmission line and inspect the power lines at a close distance. Typically, these types of robots can be separated into simple and complex designs. Simple designs are simpler in construction without much in the form of obstacle avoidance and have basic operating systems. Examples of these are shown in studies [6] and [7]. An example of a complex design is the novel tri-arm robot with dual-parallelogram architecture (DPA) developed in the study [8]. The DPA helps the movement of the arms on the robot by increasing efficiency, keeping the forces on the different arms balanced, and developing the adjacent-obstacle-crossing ability. These robots are large and have massive weights due to the multiple required parts for them to operate on.

Most power line inspection robots are for high-tension line inspection instead of residential lines that cannot support considerable weight. Moreover, the power lines in the Philippines are somewhat badly maintained in some areas. Although the status of power lines in the country is certainly better than the state of telephone wires in the country, which are sagging, knotted, and tangled, it is not uncommon to see power lines that have some form of damage. Whether this damage is dangerous to an inspector is unknown because the severity of the damage cannot be known without checking it physically. Even if some current designs are light enough for residential lines to support these robots, they usually do not have any obstacle avoidance measures or systems that are unstable and inconsistent. Therefore, existing wire-riding robots are unsuitable for residential power lines in the Philippines.

The general objective of the study is the creation of a clamshell wire-riding robot used to inspect wires and cables for damage, more specifically, residential power lines. The robot will have a weight of less than 3 kilograms in order for the robot to not place a significant burden on residential power lines. This would make the design one of the lightest power line riding robots present today, especially compared to those of [9] and [10]. The design is built on the premise that it can be constructed using 3D printing technology. The robot will be designed and simulated using tools such as Onshape, ANSYS, and SOLIDWORKS. Printing time for the robot is also considered. This study focuses on presenting a compact and lightweight wire-riding robot design that is able to traverse a variety of power/data lines. It is focused primarily on the design and simulation aspect and does not cover the actual implementation of such a design in a real-world setting. Actual testing of the physical design is covered in a separate article entitled “Fabrication and Evaluation of a Clamshell Line Inspection Robot.”

2.0 METHODOLOGY

2.1 Methodological Framework

Figure 1 below shows the methodological framework associated with the study. It starts with the design of the chassis and wheels on the basis of the clamshell concept. Afterward, the gears must be designed to accommodate the transfer of power to the powered wheel. Once the design has been fully modeled, each component can then be simulated and stress-tested in ANSYS. Assembly simulations are also performed. If the design has been deemed safe via stress simulations, motion analysis can be performed to determine the stability of the robot. The last part of the design phase is the configuration of the control and monitoring system. This section focuses more on how the robot can possibly be controlled and the type of monitoring system associated with the design.

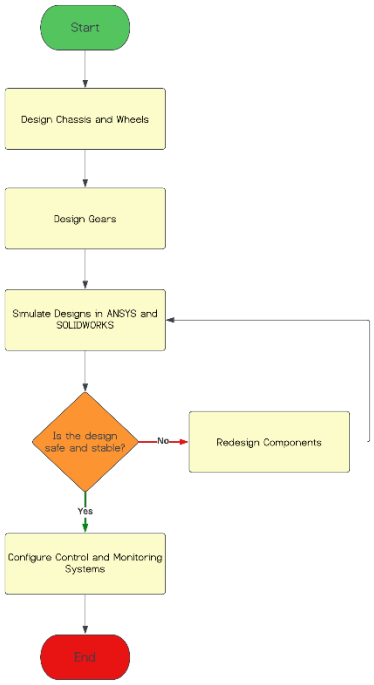

Figure 1. Methodological Framework of the Design and Testing Process

2.2 Design A Wire-Riding Robot Using A Clamshell Concept

The study aims to design a clamshell-style robot that can support its weight and navigate residential power lines. Non-conductive PLA plastic is a preferable material due to its lightweight and strength. The robot will be powered by a singular DC motor for forward motion. Previous designs utilized servo motors or DC gear motors. Motor size depends on the robot's weight and desired travel speed, aiming for 1-3 kilograms and a maximum speed of 3 km/h based on studies [9] and [10]. Battery capacity should support 20-30 rounds or 1-2 hours of operation. This is based on studies [9] and [11] which both indicate that robots of similar design or purpose last around 30 to 45 minutes before requiring a charge.

Equation 1 below shows the equation for motor torque derived in the study [12]. Here N_W stands for the number of powered wheels, D_W is the diameter of the wheels, M is the mass

of the robot, g is gravity, μ is the coefficient of rolling resistance, and a is acceleration.

$$\tau = \frac{1}{N_W} \times \frac{D_W}{2} \times (Mg\mu + Ma) \quad (1)$$

Where N_W = 1 wheel
D_W = 42.605 mm
M = 3 kg
g = 9.81 m/s²
μ = 0.002
a = 0.5 m/s²

Based on the known values, motor torque is calculated to be 0.0332 Nm. The coefficient of rolling resistance is assumed to be a constant of 0.002, based on a reference from [13]. An acceleration of 0.5 m/s² is considered, emphasizing the need for quick acceleration. Previous studies did not specify acceleration as a focal point but rather focused on top speed. Aside from torque, the required power output of the motor must be calculated. Formulas from the study [14] provide a reference of how to calculate for this and are shown in equations 2 and 3. F is the force required to move the load and the corresponding subscripts simply explain what type of force is accounted for. This force is then used to compute the power, which is in watts. Vmax is meant to signify the maximum speed the load is meant to travel.

The force required to move the robot is determined using equations 2 and 3. Equation 2 accounts for the different forces the robot encounters as it moves. There are three forces in total, which are the force of gravity, the force of friction, and the force derived from Newton's second law (F = ma). With the known variables, the force requirement is calculated to be 30.98886 N. Converting this to watts requires multiplying it by the desired speed, which in this study is set to 3 km/h. This results in a required power output of approximately 26 W.

$$F = F_{Gravity} + F_{Friction} + F_{ma} \quad (2)$$

$$P = F \times V_{max} \quad (3)$$

Where $F_{Gravity}$ = M x g
$F_{Friction}$ = M x g x μ
F_{ma} = M x a
V_{max} = 3 km/h = 0.833333 m/s

Since it is uncommon to find motors with exact specifications matching the equations, it is advisable to choose a motor that exceeds the requirements. This provides flexibility in case of neglected or incorrectly assumed variables. The motor selected for this study has a rating of 30 W and a torque rating of just under 0.1 Nm based on the specifications given in [15]. These specifications indicate that the chosen motor is more than capable of meeting the study's needs. Vibrations from the DC motor are not a significant concern, as they are unlikely to affect the robot's stability on the power line.

The equations below calculate the battery life of the robot. These are based on article [16], which presents formulas to determine the run time of a battery-powered system.

$$\frac{Watts\ Drawn}{Battery\ Voltage} = Amps\ Drawn \quad (4)$$

$$\frac{Battery\ Rating}{Amps\ Drawn} = Battery\ life\ in\ hours \quad (5)$$

Where Watts Drawn = 32.4 W
Battery Voltage = 12 V
Battery Rating = 3500 mAH

The motor has a power draw of 30 W, while the maximum power draw of an Arduino Pro Mini is around 2.4 W, according to a study [17]. Although it is unlikely for the Arduino's power draw to reach its maximum, it is considered in the calculations for caution. This results in an amp draw of 2.7 Amps. To meet the voltage requirements, a set of 18650 Lithium-ion batteries with a rated capacity of 3.5 AH according to [18] is used. Dividing the battery capacity by the amp draw yields a total run time of 1.2963 hours, which falls within the specified requirement of 1 to 2 hours of battery life.

The robot needs to be able to ride on a 14 mm² wire, which is the standard for residential drop wires, as stated by [19]. It should also be able to navigate minor obstructions. A crucial aspect is the robot's ability to transmit a clear video feed without significant vibration, as this would hinder the inspector's view. Thus, the robot must be capable of delivering a clear video feed while moving along the power line.

2.3 Various Chassis Designs

Four different chassis designs were created to test their strengths and weaknesses. The designs are seen in Figure 2, shown below. These designs were proportionate to the triplex wire to ensure proper support. The designs were limited by the parameters of the 3D printer (Ultimaker S5), but they were not restricted by printing size. The top and bottom chassis had a maximum height of 125 mm in the hexagonal design. The bottom chassis held the suspensions, while the top chassis accommodated the motor, PCB, and battery holder. The suspension here was used to increase flexibility in terms of what the robot can drive through. It allows the robot, for example, to drive over small lumps of clumped wire. Cutouts were made to position the components correctly and ensure the use of the same spur gear set for all designs. The positioning of the wheels and motor was carefully planned, and extensions on the chassis ensured a tight space for the triplex wire.

A.

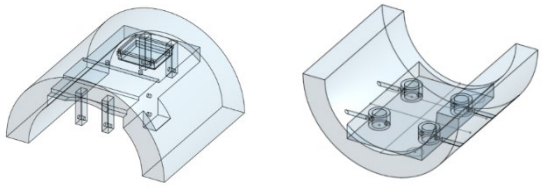

B.

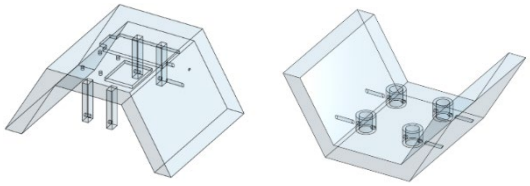

C.

D.

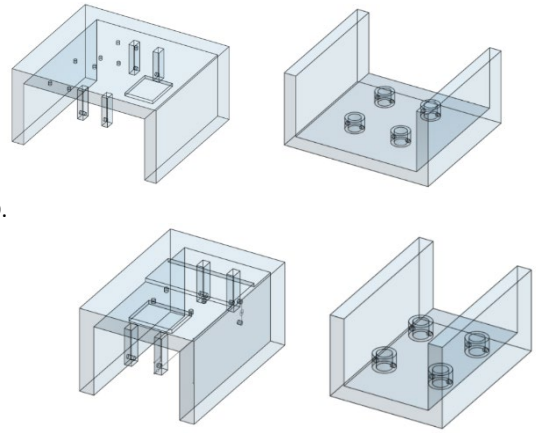

Figure 2. Chassis designs (a) Circular (b) Hexagonal (c) Wide Rectangular (d) Thin Rectangular

Initially, a circular design was conceived; however, this design came with a set of issues. Cutouts were required for better positioning of components, making maintenance and dust settlement more challenging. Printing the circular chassis also required additional support, adding time and cost.

To address the disadvantages of circular chassis, new designs were created. The wide rectangular chassis design and hexagonal chassis design offered improvements. The rectangular design provided complete structural support at the bottom, while the hexagonal design combined features of the circular and rectangular designs. The hexagonal design had flat areas for easy component placement but had uneven protrusions and cutouts that increased the risk of breakage.

The rectangular design was further divided into wide and thin variants to accommodate different wheel designs. The thin rectangular design aimed to reduce the required torque and maintain balance. It also reduced printing time compared to the wide rectangular design.

Counterbalances were added to the bottom chassis to balance the weight of the motor. These counterbalances were placed on the opposite side of the motor to balance the center of gravity and prevent the robot from flipping over during operation. Figure 3 below shows the modifications done to accommodate the counterbalances.

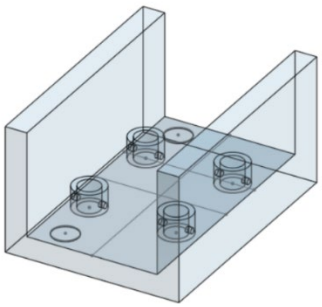

Figure 3. Thin Rectangular Bottom Chassis Designed to add Counterweights

While designing the chassis, other shapes were considered. A diamond shape was explored, which would distribute the weight closer to the center of the robot and potentially eliminate the need for counterweights. However, this design posed challenges in mounting internal components at awkward angles and lacked flat surfaces for attaching counterweights effectively. Triangular and octagonal designs were also considered but were deemed impractical due to limitations in motor mounting points or unnecessary complexity in the printing process. Ultimately, the chosen chassis design incorporated counterbalances and accounted for practical considerations to ensure balance, stability, and proper mounting of components.

2.4 Various Wheel Designs

Another point of emphasis of the design is the wheels. The wheels are an integral part of the design process as these serve as the contact points between the power line and robot. A good wheel design must be able to keep the robot stable and provide ample traction for movement. Figure 4 shows the different wheel designs presented in the study.

A.

B.

C.

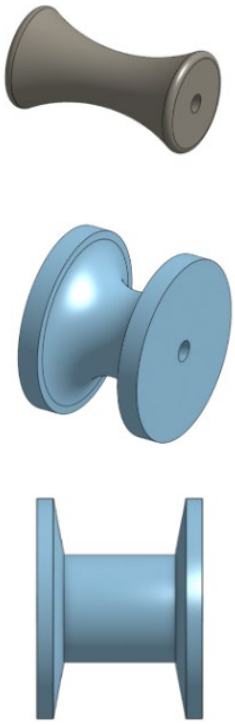

Figure 4. Wheel designs (a) Wide Wheel (b) U-type Grooved Wheel (c) V-Type Grooved Wheel

Two-wheel designs were created: the wide wheel and the grooved wheel. The wide-wheel design was initially developed to accommodate different wire diameters, allowing the wire to fit between the wheels. However, this design had limitations in terms of space utilization, lacked proper support on each side, and had a higher probability of slipping. Although the curved shape of the wheel helped reduce slipping, it was still prone to slipping off the wire.

In contrast, the grooved wheel design was specifically made to fit a specific wire diameter, reducing the chances of slipping. Side walls were added to the wheel edges to prevent rolling or falling. The design of the grooved wheel was inspired by round belt pulleys found in [20]. The catalog provided parameters such as the width of the pulley and the size of the groove relative to the belt diameter. The wheel design adapted these parameters,

with the width of the wheel being 1.5 times wider than the diameter of the wire.

The grooved wheel design further includes two variations: the U-type and V-type grooved wheels. The U-type wheel forms a curve from the center towards the groove, offering a higher contact surface area between the wire and the wheel. This additional curve increases printing time but provides structural support during the printing process. On the other hand, the V-type wheel has a sloped form, where the grooves are followed by a few millimeters of sloped printing before continuing at a constant diameter. The V-type design sacrifices the added printing time for faster printing but causes the robot to be more prone to over-rotation due to the lack of support and the lower contact area, resulting in higher pressure at the contact point.

2.5 Gearing Setup

A bevel gear design with the motor axle perpendicular to the wheel axle was considered. However, after determining the need for a different motor, a motor mounted parallel to the wheel axle was chosen instead. This required a spur gear set to transmit power from the motor to the wheel. The gear design considered the center-to-center distance between the motor and wheel axles, ensuring sufficient torque transmission. A spur gear tool was used for the 3D CAD model, specifying the module, number of teeth, and gear diameters. The gear sizes presented in the paper had 32 teeth for the gear and 23 teeth for the pinion, with a gear module of 2, resulting in a total center-to-center distance of 55mm. The model for these gears is shown in Figure 5 below.

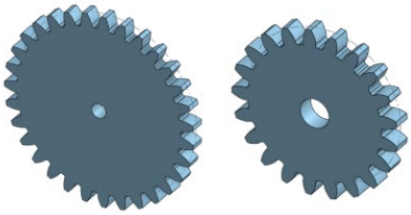

Figure 5. Spur Gear Set Up

2.6 Simulate the designs in ANSYS and SOLIDWORKS

Stress analysis using ANSYS will be conducted to ensure the reliability and performance of the robot designs. The focus will be on the wheels and chassis, as they bear the most load. Separate simulations will be performed for the wheels, applying a load to simulate the power line's weight. The top chassis and internal components will be simulated together in an assembly, as well as individually. The bottom chassis, which carries minimal weight, is of lesser concern. Additionally, motion analysis in SOLIDWORKS will be performed to observe the robot's behavior in real-world conditions. This analysis will help identify design improvements and necessary modifications to enhance performance.

2.7 Control and Monitoring System

Once the optimal design and simulation of the robot are achieved, attention shifts to the remote-control system. The system will be based on Arduino boards, consisting of a transmitter and receiver. Designs are based on [21] and [22]. A controller will be built to transmit a radio signal to an Arduino receiver, which will control the motor movement of the robot. The robot will also incorporate a camera, using a GoPro mounted outside the robot. The GoPro camera can connect to a phone via WiFi and Bluetooth, allowing for convenient monitoring [23].

3.0 RESULTS AND DISCUSSION

In this section, results from the ANSYS stress simulations and SOLIDWORKS motion analysis are presented. Included also in this section are print times derived from Cura and the approximate weights the software calculates for each component.

3.1 ANSYS Simulation Set Up

For the ANSYS simulations, the tests were split into two categories – component and assembly simulations. The purpose of splitting these tests was to observe and measure the performance or structural stability of the design as a single entity and complete the design with all the components attached to it. The component simulations had a 5 kg load placed to act as the overall weight of the robot as well as any additional loads that the robot may unexpectedly experience during operation. A fixed support was placed either on the contact point of the wheel or the axel mounting points of the chassis. The assembly simulations had similar boundary conditions; however, the load was increased to 10 kg to simulate the extra weight and stress by the internal components. All tests used adaptive sizing mesh and the maximum number of elements permitted with the student license of ANSYS to ensure maximum accuracy. Each model is 220 mm in length, 115 – 125 mm in height, and 160 – 250 mm in width. The material used in the simulation was PLA plastic, which in ANSYS has a yield strength of 54.1 MPa. Figure 6, shown below, illustrates the component and assembly simulations performed in ANSYS.

A.

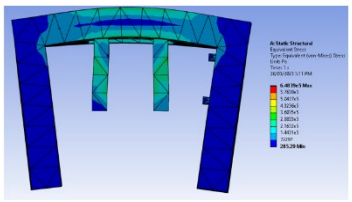

B.

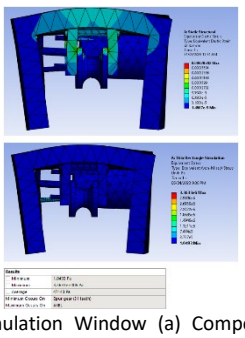

Figure 6. ANSYS Simulation Window (a) Component Simulation (b) Assembly Simulation

3.2 ANSYS Simulation Results

As seen with the results in Table 1 below, the highest equivalent stress was experienced with the hexagon top chassis due to the large extrusion made to attach the motor; however, all the designs were found to have a large margin of error with a safety factor of 15 across all the simulations. Note that ANSYS labels von-Mises Stress as Equivalent Stress. Considering how low the von-Mises Stress is, it is understandable why the safety factor is 15. If the yield strength were to be taken and divided by each of the stresses, each safety factor would be in excess of 15. ANSYS simply does not compute safety factors greater than 15. The total deformation refers to the square root of the deformation summation on all three axes. It gives a general approximation of the area of the robot that encounters the most deformation. If a portion of the robot deforms to such an extent, it may render the robot inoperable.

Table 1. Initial Chassis Simulations

Part	Highest Equivalent Stress (Pa)	Total Deformation (m)
U-Grooved Wheel	4.307e5	1.169e-6
V-Grooved Wheel	3.340e5	1.158e-6
Thin Rectangle Top Chassis	6.484e5	6.425e-7
Hexagon Top Chassis	3.327e6	1.990e-6
Cylinder Top Chassis	7.694e5	7.818e-7
Part	**Highest Equivalent Stress (Pa)**	**Part with Highest Stress**
Thin Rectangle	3.363e6	Wheel Axel
Hexagon	2.581e6	Top Chassis
Cylinder	3.607e6	Wheel Axel

An additional 5kg was added to make a total 10kg load for the assembly simulations, to further test the capability of the design. However, once again, all the assemblies were found to have a large safety factor overall, with a simulation result of 15 across all the chassis assemblies. However, it is notable that for the hexagonal design, the top chassis carried the largest stress, once again due to the large extrusion made for the motor mounting point. Regardless, it is evident that there is a large margin of error for the application of an infill structure during the 3D printing process. This was likely a result of the thickness of the chassis and its density. The chassis did not have a set infill percentage, and as a result, they were fully filled in the simulations. Knowing this, however, gave the researchers of this study the confidence to reduce the infill percentage due to the high factor of safety.

3.3 Cura Weights and Print Times

Table 2, shown below, presents the approximate printing times and weights of the different smaller components associated with the robot. This was calculated through Cura, the software associated with the Ultimaker S5. It involved uploading the 3D models of the components into the software, which displays the approximate printing time and weight of the part. As observed in the table, the U-type wheel takes marginally more time to print than the V-type wheel; however, this difference was not considered to be significant enough to discount the U-type wheel as a reasonable design. Instead, it was decided that the wheel choice would be a result of their performance during the motion analysis. Overall, the printing time for all components was considered to be within reason.

Table 2. Component Printing Times and Weight

Printing Times (Components)		
Part	**Engineering**	**Weight**
U-Grooved Wheel	2h 5min	14g
V-Grooved Wheel	1h 54min	13g
Bevel Gear Set	1h 39min	11g
Spur Gear Set	2h 27min	18g

Figure 7 shows a Cura printing simulation of the thin rectangular chassis. In the software, it shows different print settings that are available. Both the draft setting and engineering settings were used for the purposes of estimating print times and weights for the chassis designs. This was done with a 10% infill setting which was deemed acceptable due to the high factor of safety. On the bottom hand corner is the estimated print time and weight of the model.

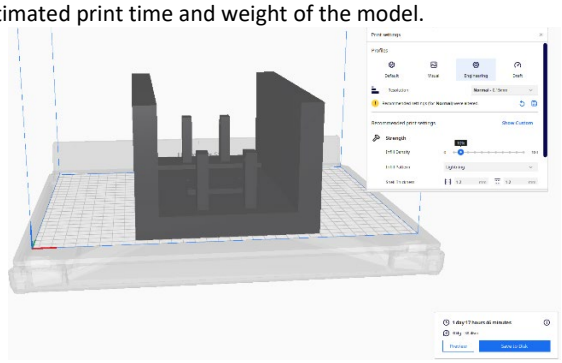

Figure 7. Cura Printing Simulation

Table 3 shows the printing times for all the different chassis. The table clearly shows that all the designs had rather high printing times. Even when the draft setting was used, the printing times still were close to, if not exceeded the duration of a whole day. This is often to be expected when 3D printing complex parts. It is worth noting that the design that took the least approximate time to print was the thin rectangular design. The draft print setting was also not considered to be a realistic and suitable print setting.

Table 3. Chassis Printing Times and Weights

Printing Times (Top and Bottom Chassis)			
Part	**Engineering**	**Draft**	**Weight (E/D)**
Thin Rectangle	3d 11h 32min	20h 55min	611g/447g
Hexagon	3d 22h 46min	1d 3h 28min	679g/480g
Cylinder	4d 8h 52min	1d 7h 29min	719g/515g
Wide Rectangle	4d 5h 51min	24h 28min	742g/539g

3.4 SOLIDWORKS Motion Analysis Set Up

Figure 8 below shows the different physical elements of the motion analysis study. It is comprised of an electric pole,

insulator, and triplex wire. The model includes two poles, in which an insulator is used to mount the triplex wire.

The robot was then mounted onto the wire, using the wheels as the contact points between the robot and the wire. Note that the whole robot could have been modeled to have contact with the wire; however, this would have been inefficient and unnecessary as the focus of the motion analysis is the contact between the wheels of the robot and the wire. Despite this, the weight of each component is still considered in the study. Each individual component plays a major factor in the center of mass of the robot, especially considering its small size. The bottom suspension was also modeled in the experiment using the in-built spring parameter feature. This allows the bottom row of wheels to be flexible and not rigid, similar to how it would behave in real life. A motor function with an RPM of 200 was set on the powered wheel to simulate the effect of a motor on the robot. This allowed the robot to move along the power line so that its behavior could be monitored while in motion. No force apart from gravity was applied to the system.

A.

B.

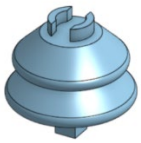

C.

Figure 8. Moton Analysis Components (a) Post (b) Insulator (c) Triplex wire

3.5 SOLIDWORKS Motion Analysis Results

The figures 9 shown below show the behavior of each design with and without counterweights. All designs would tip over to one side due to the weight of the motor. In order to counteract this, weights were added to the opposite side to keep the robot upright. A noticeable improvement in terms of stability was observed afterward for all designs. The application of the V-type wheel is also seen at the bottom of Figure 9a. It was observed that this wheel would make the robot more unstable than the U-type wheel. The wide wheel design shown in Figure 5b also yielded negative results, with the robot unable to traverse the power line due to the lack of support from the wheels. All subsequent designs that used U-type wheels performed relatively similarly in terms of stability. The most notable designs from the simulations are the thin chassis and the cylindrical chassis. Both performed well in terms of stability, making the deciding factor for which design to proceed with the 3D printing time. The thin rectangular chassis takes less time to print and is a preferable shape to 3D print, mainly due to the fact that curved surfaces are not preferable when it comes to 3D printing.

A.

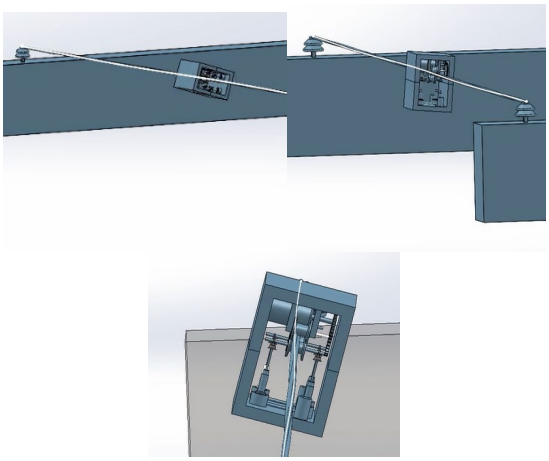

B.

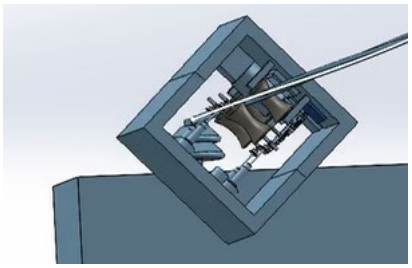

C.

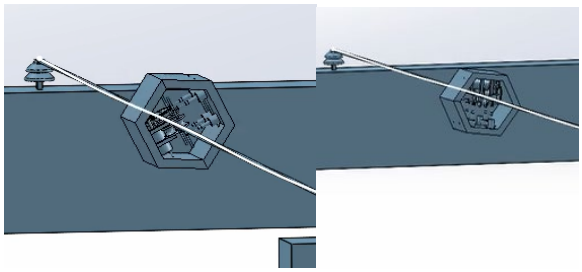

D.

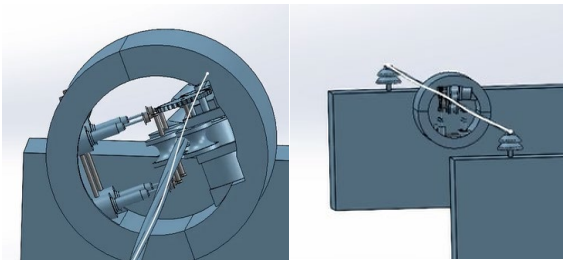

Figure 9. Chassis designs (a) Thin Rectangular (b) Wide Rectangular (c) Hexaonal (d) Circular

3.6 Modified Final Design

Now, knowing what shape is optimal, a greater effort to reduce printing time and costs was pursued. Figure 10 shows a truss design that was made in consideration to further reduce the printing time to be able to print each part of the chassis within a day. This was done through the truss design that would affect

the printing process by cutting the time needed to almost half of the previous printing time while keeping most of the structural integrity. A truss design is a term mainly used when building bridges. It allows for the distribution of load via the diagonal members of the structure. In this case, it permits material to be removed from the chassis while still maintaining the structural rigidity of the chassis. The thickness of the overall chassis was also halved to 10 mm. Mounting points for certain components were also added to the design to remove the need for drilling holes, which could compromise the structure of the chassis.

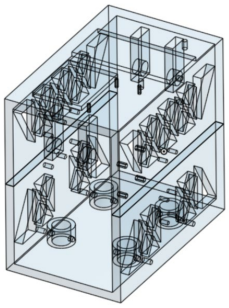

Figure 10. Chassis with Truss Design

Using a similar simulation setup the added holes added into the chassis were still able to withstand the expected forces experienced by the robot during operation. As seen in the ANSYS component simulations, a safety factor of 15 was observed, which provides a margin of error in the case of any additional forces occurring during operation. The biggest notable change was with the printing times and component weights (Table 4). A modified draft setting more suited for the application was used and resulted in print times greater than that of the original draft setting but significantly less than that of the engineering setting. This setting also ensures the structural integrity of the chassis, meaning that the print time was reduced from 3 days to just over 1 day in total. The weights of each chassis were also more than halved. The print setting made use of a layer height of 0.3 mm, wall thickness of 0.8 mm, triangular infill density of 10%, and a skirt build plate adhesion type.

Table 4. Revised Chassis Simulations

Component Simulations			
Part	**Highest Equivalent Stress (Pa)**	**Total Deformation (m)**	**Safety Factor**
Thin Top Chassis with Trusses	2.6646e5	5.4225e-5	15

Printing Times			
Part	**Engineering**	**Modified Draft**	**Weight (E/D)**
Top Chassis	2d 4hrs 31mins	12hrs 27mins	381g/267g
Bottom Chassis	2d 5hrs 3mins	12hrs 33mins	390g/268g

Figure 11 below shows the behavior of the revised design in SOLIDWORKS. Based on the results, the design behaved roughly the same as the original design it was based on. From this it can be concluded that the revised design should be capable of both managing the weight of the components and the loads it may experience and stable enough so that a line inspection can be performed without too much unwanted and unnecessary motion. Based on this design, the projected total weight of the robot without counterweights is under 1.5 kg in total.

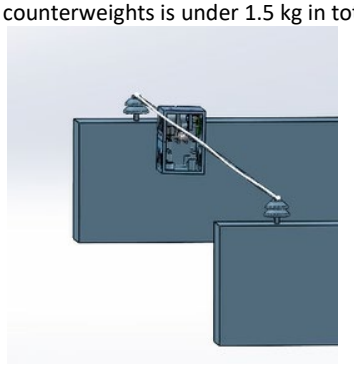

Figure 11. Revised Design Behavior

4.0 CONCLUSION

This research presented the concept of a clamshell power line riding robot and a possible design for it considering the weight, speed, and battery life parameters based on previous studies. The study presents several different chassis designs for the application, namely a thin and wide rectangular chassis as well as cylindrical and hexagonal designs. Different designs exploring various shapes and widths for the wheels were also analyzed.

Stress testing the different chassis and wheel designs in ANSYS yielded exemplary results for all designs, indicating that all designs for both the wheels and chassis would not break under load. All parts had a safety factor of 15, which gives allowance to reduce the infill percentages on the 3D printed structure.

Among the different designs, it was found that the thin rectangular design and the cylindrical chassis using the U-type grooved wheels were the most stable designs observed using SOLIDWORKS motion analysis. Both designs performed relatively similarly, meaning that the deciding factor between the two designs was the print time.

Based on the data from the Cura software, the thin rectangular chassis takes less time to print. With this in mind, more effort needed to be made to reduce print time, which was over 3 days with the applicable print setting. A truss design with a thinner chassis was run through ANSYS stress testing and was found to have performed satisfactorily. A motion analysis with the same design found that it performed and behaved the same as the original design. The print time was reduced to just over 1 day, and the weight of the design was cut in half. The total weight of the robot is under 1.5 kg, with the projected battery life of the robot exceeding 1 hour at an estimated inspection speed of 3 km/h.

The design's main advantage over existing designs is its simplicity, reducing the robot's weight and increasing its flexibility. The clamshell design improves weight distribution, making movement on the power line smoother and reducing strain. The compact design places all main components inside the robot, eliminating protruding parts. The 3D-printed clamshell reduces weight compared to heavy metal parts and minimizes the need for additional links or joints. Overall, the clamshell design addresses critical issues faced by current power

line riding robots, making it more suitable for residential power lines.

Acknowledgement

The researchers of this study would like to extend their sincerest thanks and gratitude to the Department of Mechanical Engineering of De La Salle University – Manila, Philippines, for their support and for providing the resources needed to complete this research.

Conflicts of Interest

The author(s) declare(s) that there is no conflict of interest regarding the publication of this paper

References

[1] Huawei. 2023. Intelligent Transmission Line Inspection Solution. [Online] Available: https://e.huawei.com/en/industries/grid/power-grid/transmission-line-intelligent-inspection. Accessed May 2023.

[2] D. J. Friedman, 2014. "Electrical Safety Hazards and Safe Electrical Inspection Procedures for Electrical Inspectors & Home Inspectors. "https://inspectapedia.com/electric/Electrical_Inspector_Safety.php (accessed Oct. 16, 2022).

[3] Power Magazine, 2020 "The past, present, and future of Powerline Inspection Automation," Sep. 18, 2020. https://www.powermag.com/the-past-present-and-future-of-powerline-inspection-automation/ (accessed Oct. 16, 2022).

[4] S. Hrabar, T. Merz, and D. Frousheger, 2010. "Development of an autonomous helicopter for aerial powerline inspections," in *2010 1st International Conference on Applied Robotics for the Power Industry, CARPI 2010*, doi: 10.1109/CARPI.2010.5624432.

[5] W. Chang, G. Yang, J. Yu, Z. Liang, L. Cheng, and C. Zhou. 2017. Development of a Power Line Inspection Robot with Hybrid Operation Modes. *International Conference on Intelligent Robots and Systems. Vancouver: IEEE.* doi: 10.1109/IROS.2017.8202263.

[6] A. Fonseca, R. Abdo, and J. Alberto. 2012. Robot for inspection of transmission lines. *2nd International Conference on Applied Robotics for the Power Industry. Zurich: EEE Computer Society*. 83–87. doi: 10.1109/CARPI.2012.6473356.

[7] M. A. Gulzar, M. Sharif, K. Kumar, and M. A. Javed. 2018. High-Voltage Transmission Line Inspection Robot. *2018 International Conference on Engineering and Emerging Technologies (ICEET). Lahore: IEEE.* doi: 10.1109/ICEET1.2018.8338632.

[8] D. Yang, Z. Feng, X. Ren, and N. Lu. 2014. A novel power line inspection robot with dual-parallelogram architecture and its vibration suppression control. *Advanced Robotics*. 28(12): 807–819. doi: 10.1080/01691864.2014.884936.

[9] P. Debenest and M. Guarnieri. 2010. Expliner - From prototype towards a practical robot for inspection of high-voltage lines. 1st International Conference on Applied Robotics for the Power Industry. Montreal: IEEE. Doi: 10.1109/CARPI.2010.5624434.*Conference on Applied Robotics for the Power Industry, CARPI 2010,* 2010. doi: 10.1109/CARPI.2010.5624434.

[10] Y. G. Wang, H. D. Yu, and J. K. Xu. 2014. Design and simulation on inspection robot for high-voltage transmission lines. *Applied Mechanics and Materials.* 615: 173–180. doi: 10.4028/www.scientific.net/AMM.615.173.

[11] droneblog. 2020. How Long Does a Drone Battery Last? What You Need to Know! [Online] Available: https://www.droneblog.com/how-long-does-a-dronebattery-last-what-you-need-to-know/#:~:text=The%20typical%20flight%20time%20for,between%2020%20to%2030%20minutes. Accessed April 2023.

[12] A. H. Ali, S. M. H. Kazmi, H. A. Poonja, H. Khan, M. A. Shirazi, and R. Uddin. 2022. Motor Parametric Calculations for Robot Locomotion. *Engineering Proceedings*. 20(1): 1–5, doi: 10.3390/engproc2022020008.

[13] R. Kurtus. 2016. Coefficient of Rolling Friction. [Online] Available: https://www.school-for-champions.com/science/friction_rolling_coefficient.htm#.ZDd_yHZBy3A. Accessed April 2023.

[14] M. K. Gönüllü. 2013. Development of a Mobile Robot Platform to Be Used in Mobile Robot Research. *Middle East Technical University*. 1: 16–18.

[15] Handson Technology. 2019. 3420 Dual Ball Bearing Long Life DC Motor. [Online] Available: https://handsontec.com/dataspecs/motor_fan/XD3420-Motor.pdf. Accessed June 2023.

[16] Newport Vessels. 2021. Trolling Motor Run Time: How to Calculate Run Time. [Online] Available: https://newportvessels.com/blogs/resource/calculate-motor-run-time#:~:text=Motor%20amperage%20draw%20describes%20how,it%20by%20the%20amperage%20draw. Accessed April 2023.

[17] S. Thornton. 2020. Microcontroller power source considerations for Arduino. [Online] Available: https://www.eeworldonline.com/microcontroller-power-source-considerations-arduino/. Accessed April 2023.

[18] LiitoKala. 2019. Lii-35A. [Online] Available: http://www.liito-kala.com/page92?product_id=13. Accessed June 2023.

[19] Philflex. 2020. Service Drop Cable (Triplex). [Online] Available: https://www.philflex.com/_files/ugd/8be76e_909372397733428ea8349900634c3b74.pdf. Accessed November 2022.

[20] McMaster-Carr. 2020. Round-Belt Pulleys. [Online] Available: https://www.mcmaster.com/pulleys/for-belt-type~round/. Accessed April 2023.

[21] D. Nedelkovski. 2019. DIY Arduino RC Transmitter. [Online] Available: https://howtomechatronics.com/projects/diy-arduino-rc -transmitter/. Accessed June 2023.

[22] D. Nedelkovski. 2020. DIY Arduino RC Receiver for RC Models and Arduino Projects. [Online] Available: https://howtomechatronics.com/projects/diy-arduino-rc-receiver/. Accessed June 2023.

[23] GoPro. 2022. HERO11 Black. [Online] Available: https://gopro.com/en/us/shop/cameras/hero11-black/CHDHX-111-master.html. Accessed September 2022.